Bulletin of the Seismological Society of America, Vol. 77, No. 5, pp. 1674–1687, October 1987

OBSERVATION OF A REFLECTION FROM THE BASE OF A MAGMA CHAMBER IN LONG VALLEY CALDERA, CALIFORNIA

BY JOHN J. ZUCCA, PAUL W. KASAMEYER, AND JOSEPH M. MILLS, JR.*

ABSTRACT

Lawrence Livermore National Laboratory deployed a small network of 14 three-component digital seismographs during August 1982 in the Mono Craters area, which is located just north of Long Valley caldera. The network recorded small earthquakes located to the south of Long Valley. One event shows a clear arrival between the *P* and *S* phases, which is interpreted as a reflected phase similar to that observed by other researchers in the Long Valley area. The reflected phase follows the *P* arrival by approximately 4.3 sec and has an apparent velocity of approximately 7.0 km/sec. Particle motions indicate that the reflection arrives at the surface as a *P* wave. Travel-time, amplitude, and particle motion modeling of the *P*, *S*, and reflected waves suggest that the reflected phase is best modeled as a *P* to *P* reflection from the base of a low-velocity layer. The layer is approximately 19 km thick and has a velocity contrast of 17 per cent with the basement rocks. The low-velocity layer extends to the lower crust and is floored with high-velocity (greater than 7.0 km/sec) material. A zone of partial granitic melt underlain by higher velocity basaltic rocks could account for the computed velocity structure.

INTRODUCTION

Long Valley has been a continuing source of silicic volcanism for over the last 2 m.y. (Bailey *et al.*, 1976). In recent years, it has also been the site of intense earthquake activity. Two major swarms have occurred, one in May 1980 (Archuleta *et al.*, 1982) and the other in January 1983 (Pitt and Cockerham, 1983). Both swarms had several events with magnitudes over 5. This seismicity occurred concurrently with inflation of the resurgent dome inside the caldera by more than 30 cm since 1979 (Savage and Clark, 1982). Because this recent activity may reflect both potential volcanic hazards and the potential of the region for geothermal power production, it has rekindled scientific interest in Long Valley.

Knowledge of the deep structure of Long Valley comes primarily from seismic studies. Johnson (1965), Eaton (1966), and Prodehl (1979) conducted the early reconnaissance work in the area with long-range seismic refraction profiles. Studies since then have found evidence, in the form of low-velocity layers (LVL) and low-*Q* regions, for the existence of magma or partially molten rock beneath the caldera. Hill *et al.* (1985a) summarize the data delineating upper parts of that magma body. Hill (1976) observed an arrival branch on a seismic refraction profile that he interpreted to be a reflection from the top of a magma chamber which was duplicated in a later work (Hill *et al.*, 1985a). Ryall and Ryall (1981), Sanders and Ryall (1983), and Sanders (1984) have examined *S*-wave attenuation patterns from regional and local earthquakes and have found evidence for an extensive system of magma chambers under Long Valley. Hauksson (1985) has observed depletion of high-frequency seismic energy in the area around the resurgent dome, which he interprets as evidence for magma. Most recently, Rundle *et al.* (1985, 1986) have used an

* Present address: Sohio Petroleum Company, Geophysical Research and Development, 5400 LBJ Freeway, Suite 1200, Dallas, Texas 75080.

assortment of seismic techniques in concert to prospect for magma beneath Long Valley and to propose a site for a deep drill hole to the top of the magma chamber.

Most of these efforts, however, have focused on delimiting the top of the inferred magma chamber. In this paper, we present evidence on the location of the bottom of the magma chamber. Two other studies have provided information about the depth to the bottom of the magma chamber. Steeples and Iyer (1976) inferred from teleseismic *P*-wave delays that low-velocity material extends from 7 km depth to 25 to 40 km, depending on the velocities assumed. Luetgert and Mooney (1985) have examined seismic refraction data from earthquake sources and have identified a reflection that appears to be from the lower boundary of a magma chamber. They detected the reflection with a linear array of single-component stations, and assuming it traveled in a vertical plane, matched the travel time and apparent velocity (6.3 km/sec) to deduce that it was a $P - P$ reflection from within an LVL. We recorded a similar phase with a two-dimensional array of three-component stations and perform a similar analysis, but utilize additional information about the travel path, particle motions, and amplitudes to constrain our interpretation.

Our data come from a passive seismic refraction experiment which Lawrence Livermore National Laboratory conducted during the first half of August 1982. The purpose of the experiment was to investigate crustal structure in the region and to relate this structure to magmatic processes. Fourteen portable seismograph stations were deployed in a network with approximately 5 km station spacing in the Mono Craters region north of Long Valley (Figure 1). The network recorded earthquakes located south of Long Valley and in the south moat. The stations consisted of digital seismographs which used 1 Hz seismometers. Three components of motion were recorded at all sites, including at A1 and A2 where small (340 m station spacing) four-station arrays of vertical-component seismographs were deployed along with the three-component stations. The data represent one of the few times that three-component data have been collected for ray paths through a magma chamber in the Long Valley area.

Data

The array operated in an individual station-triggered mode. Although more than 100 events were recorded by elements of the array, only the three earthquakes shown in Figure 1 triggered a large portion of the array. The locations of the events were calculated from the Mammoth Subnetwork of the U.S. Geological Survey Calnet (R. Cockerham, written communication, 1984). Table 1 lists the summary cards for these events.

Figure 2 shows the vertical-component record sections for the three events. Radial and transverse components were also recorded, but are not shown here. The three record sections have different characters. All show the *P* arrival quite clearly, but only EQ1 and EQ3 show a clear *S* arrival. Although the horizontal component data are not shown, they mirror the observations on the vertical-component data, including the lack of a clear *S* arrival from EQ2. For EQ1, a very prominent arrival occurs between the *P* and *S* arrivals. We call this arrival the *Pr* arrival after the notation used in Luetgert and Mooney (1985). There is also a faint suggestion that the *Pr* arrival exists from EQ3 (Figure 2C). Note that the solid lines in Figure 2 show correlations only; they do not represent computed travel times from a model.

The relative amplitude relationships of the *Pr* phase are important. Inspection of Figure 2, A and C, shows that, at the traces where *Pr* is observed, the *P* arrival is the smallest amplitude, the *Pr* arrival is the next largest, and the *S* arrival is the

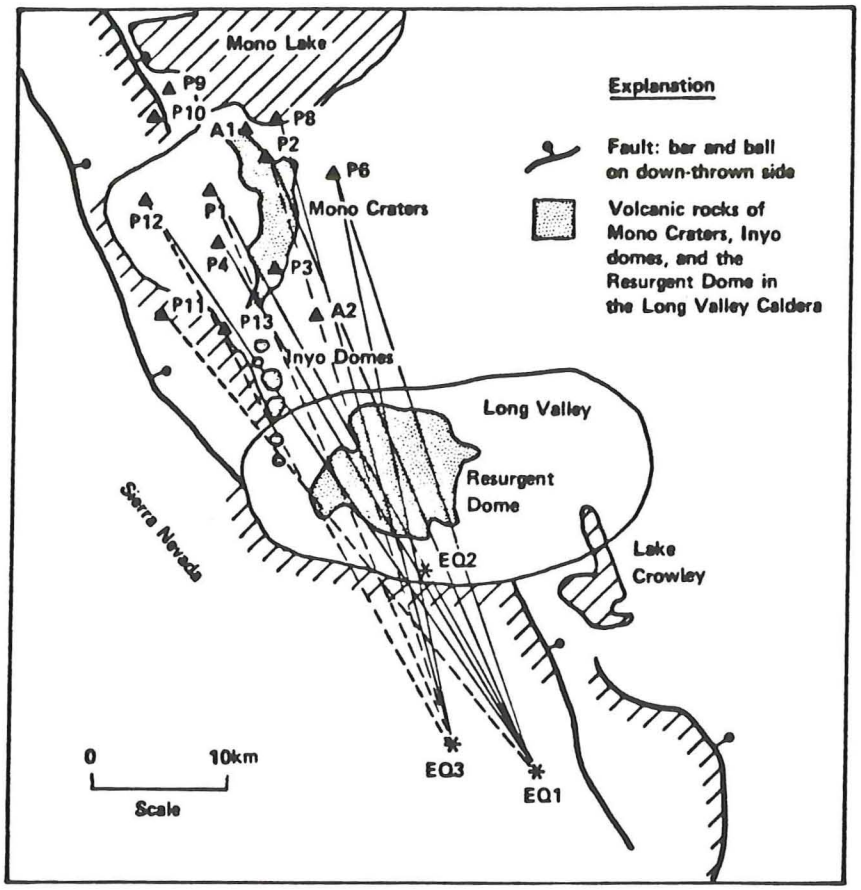

FIG. 1. Regional geology and locations map for the Lawrence Livermore National Laboratory 1982 passive seismic experiment. Solid and dashed lines radiating from EQ1 and EQ3 show along which path the *Pr* arrival is observed and not observed, respectively.

TABLE 1

SUMMARY CARDS FROM U.S. GEOLOGICAL SURVEY LOCATIONS FOR EVENTS USED IN THIS STUDY*

Event Name	Origin Time			Latitude	Longitude	Depth	Magnitude	No.	Gap	DM	RMS	ERH	ERZ	Q
	y m d	h m	s											
EQ1	820809	340	9072	37-28.53	118-48.51	6.21	2.74	8	127	12.9	0.07	0.5	2.3	C1
EQ2	820805	1538	30.49	37-36.87	118-54.04	2.76	3.55	21	93	1.4	0.14	0.5	1.1	B1
EQ3	820805	6 9	38038	37-29.76	118-52.61	2.06	3.49	8	132	11.5	0.19	1.426	5.0	C1

* For a complete explanation of variable meanings, see Lee and Lahr (1975).

largest. In Figure 2C, *Pr* is observed with confidence only at stations P6 and P8. This information provides important constraints on the modeling discussed in a later section.

The *Pr* phase is probably not due to energy from an event other than EQ1 for the following reasons. The apparent velocity of *Pr* is approximately 7.0 km/sec, which is too high for it to be the *P* arrival from another local event. Furthermore, there is no corresponding *S* arrival observed later in the record, even out to 25 sec after *P* (not shown).

Our data and the Luetgert and Mooney (1985) data are similar in travel-time and

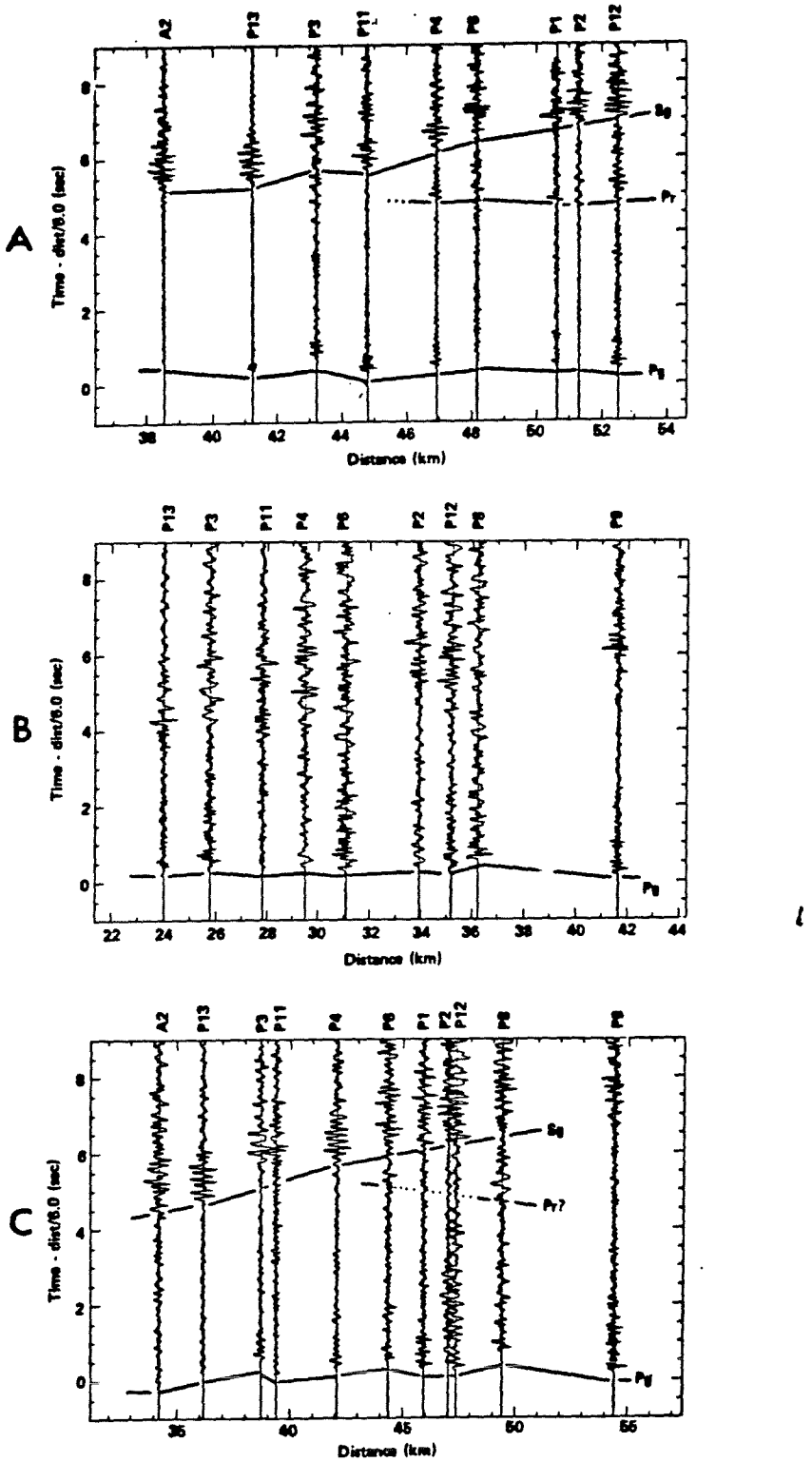

FIG. 2. Record sections of vertical components for (A) EQ1, (B) EQ2, and (C) EQ3. The sections are plotted in a trace-normalized format and are reduced to 6 km/sec.

amplitude relationships, but they obtained more consistent recordings of *Pr* and observed it from at least seven events. There is a major difference, discussed more below, in the two data sets. Our *Pr* phase arrives much later than that of Luetgert and Mooney and has a 10 per cent higher apparent velocity. We are confident that we are observing some sort of reflected phase, but the reflector is deeper than that studied by Luetgert and Mooney.

Particle Motions

We used particle motions and array processing to answer two important questions about the data: first, does *Pr* arrive at the surface as a *P* or *S* wave? This is an important question since the earlier study of these reflected phases recorded vertical-component data only, and it is not certain that the phases are *P* waves. Second, does *Pr* travel in the vertical plane between the network center and the event or has it been laterally refracted through the high-velocity Sierran basement to the west? Since the deployment is two-dimensional and all three components of motion were recorded, we are able to address these questions. Figure 3 shows the seismograms and particle motions for *P* and *Pr* at station P4 which recorded a good signal. On the vertical versus radial component plot, note that *P* and *Pr* exhibit similar behavior except that *Pr* arrives at a much steeper angle, which indicates that *Pr* indeed arrives at the station as a *P* wave. Inspection of the radial versus transverse component plots suggests that both *P* and *Pr* arrive off-axis from the west. This same result was obtained for most of the other stations recording EQ1. However, by treating the network as an array and fitting a plane wave to the *Pg* and *Pr* arrivals, we see that the energy traveled straight from the source to the stations. The distance from EQ1 to the network center is approximately three times the width of the network, so the plane wave approximation is valid and in fact the residuals are quite small (approximately 0.05 sec). The solution for the best-fit plane wave provides the apparent velocity and angle of approach of each wave. The results of this calculation for both *P* and *Pr* suggest that they arrive within 2° of the backazimuth. An explanation for this apparent contradiction is that particle motions can be severely effected by near-surface structure, but the plane-wave analysis should reflect the overall travel of the wave.

Combining the above observations, we conclude, as Luetgert and Mooney (1985) had done for their data, that the *Pr* phase arrives at the array as a *P* wave and has sampled deeper in the crust than *P*, because of the steeper angle of incidence. Furthermore, neither *Pg* nor *Pr* has been significantly refracted laterally. In the next section, we will use a two-dimensional method to model the data, with the solution constrained by the fact that *Pr* must arrive at the surface as a *P* wave.

Modeling

In the modeling which follows, we attempt to explain four sets of observations discussed above. The first is the travel times of *Pg*, *Pr*, and *Sg*. The second is the angle of incidence data from the particle motion analysis. The third is the relative amplitudes of the *Pg*, *Pr*, and *Sg* arrivals, and the fourth is the areal variability of the *Pr* arrival. Our data set is admittedly limited and therefore we present three alternative models which limit the possible seismic structures in the area. We also limit our formal modeling only to the EQ1 data, since it is the most complete record section.

To model the data, we used the Computer Program SEIS81 (Červený and Psencik, 1981) which allows raytracing of both *P* and *S* waves through two-dimensional

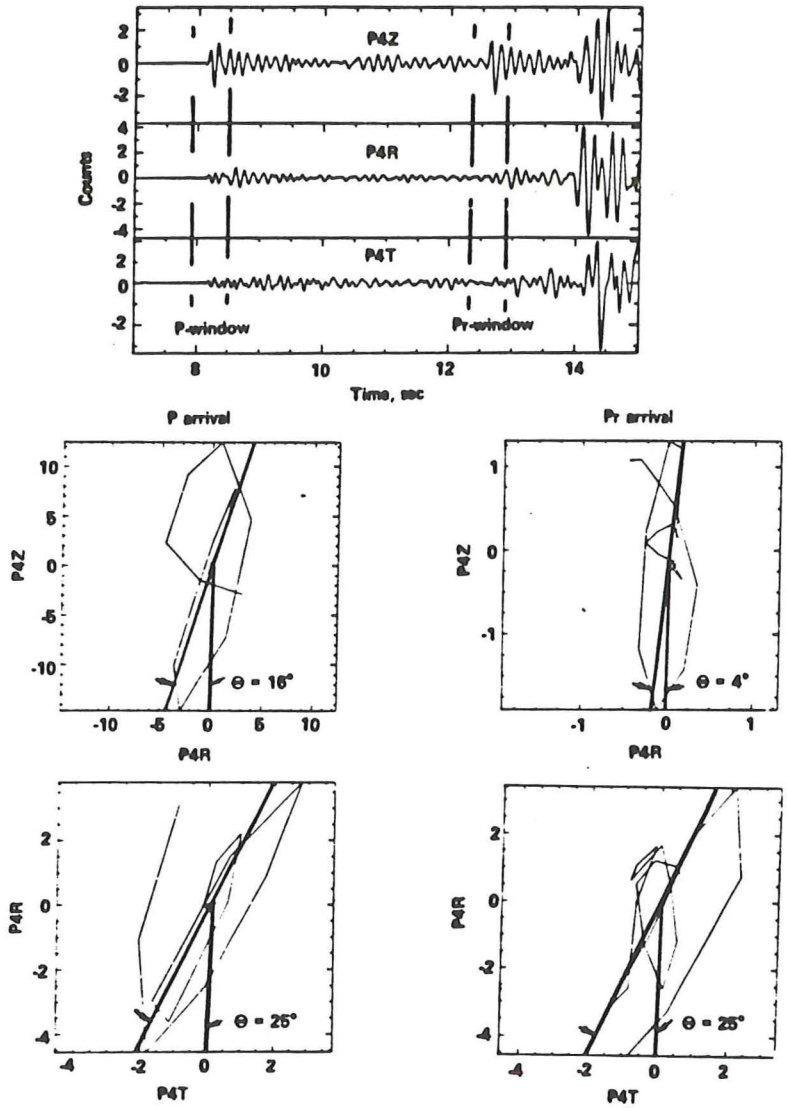

FIG. 3. Particle motions for the *P* and *Pr* arrivals at station P4 of EQ1.

media. The uppermost part of the model is not constrained by our data. Instead, we fixed the structure above 5 km depth by using the Hill *et al.* (1985a) analysis of a U.S. Geological Survey seismic refraction profile that is nearly coincident with our profile. Error in location of the earthquake will not significantly influence the results of the modeling to be presented. A change in depth of the epicentral location would change the computed travel time a few per cent but would not change apparent velocities and amplitude relationships.

SEIS81 has a provision to include a radiation pattern for *P* and *S* waves. We attempted to compute a fault plane solution for EQ1 using our data combined with data from the U.S. Geological Survey permanent network. Although a strike-slip solution fit the data, there was too much uncertainty in the solution to include it here. Archuleta *et al.*'s (1982) study of seismicity south of Long Valley found that a mostly strike-slip focal mechanism was appropriate for the large portion of the

events that they recorded. For the purposes of our modeling, then, we assume that EQ1 possesses a strike-slip focal mechanism. This assumption simplifies the modeling because the actual orientation of the nodal planes is not important. At a given azimuth and take-off angle from the event, the absolute P and SV wave amplitudes vary with the nodal plane strike, but the ratio between P and SV amplitudes remains constant.

This can be seen by evaluating the far-field terms in the radiation pattern from a shear dislocation for a dip of 90° and a rake of 0° [Aki and Richards (1980), equations (4.84) and (4.85)]

$$F^P = \sin(2\Delta\phi)\,\sin^2(i_P)$$

$$F^{SV} = \tfrac{1}{2}\sin(2\Delta\phi)\,\sin(2i_S).$$

Here, F^P and F^{SV} are the relative amplitudes of the P and SV waves, $\Delta\phi$ is the difference in azimuth of the fault plane strike and the ray path and i_S and i_P are the take-off angles of the different rays. Hence, the amplitude ratio for the two rays at the same azimuth depends only on their take-off angle with respect to horizontal and not on the azimuthal angle relative to the strike. Therefore, the simple assumption that the event was strike slip is all that is necessary for our amplitude ratio modeling. If the event were not strike slip, we would have to know the focal mechanism very well to do any amplitude modeling.

All three models presented here provide a good match to the travel-time data. Travel-time data are the primary quantity in refraction seismology and must be matched before the secondary data, amplitudes, and incidence angles can be considered. The secondary data allow us to eliminate many models.

A one-dimensional model without a low-velocity zone fits the travel-time and incidence angles. In the model shown in Figure 4D, which is based on regional velocity structure reported by Prodehl (1976), *Pr* is a simple *PmP* reflection. In this case, the travel times and angles of incidence data are well-matched but the *Pr* arrival amplitude is approximately one-tenth the size of *Pg* arrival amplitude. Prodehl's regional velocity structure matches the travel-time data much better than a model based on the regional seismic refraction work of Eaton (1966).

A critical or postcritical reflection from a high-velocity contrast boundary can produce the observed amplitudes. The second model, which has an extensive LVL, is shown in Figure 4, A to C, along with travel times from EQ1. This model matches the amplitude information quite well, but does not satisfy the particle motions. The angles of incidence for *Pg* and *Pr* from the data are 16° and 4°, respectively. We calculated the synthetic particle motions by computing the radial synthetic seismogram. The calculated synthetic particle motions are 15.5° and 13° for *Pg* and *Pr*, respectively.

Two-dimensional models, such as the one shown in Figure 5, appear to provide the best fit to the data. This model is based on a LVL centered under Long Valley and Mono Craters. For this model, several features were arbitrarily fixed. The top of the LVL was assumed to be horizontal and fixed at 7.5 km depth below the receivers. The southern boundary was held at the caldera boundary and set to be almost normal to the ray paths at that point. The thickness and velocity in the LVL trade-off and are poorly constrained; for this model, we set the velocity at 5.0 km/sec. With those assumptions, the depth and tilt of the reflector at the base of the LVL is determined from the average *Pr* travel time and angle of incidence for

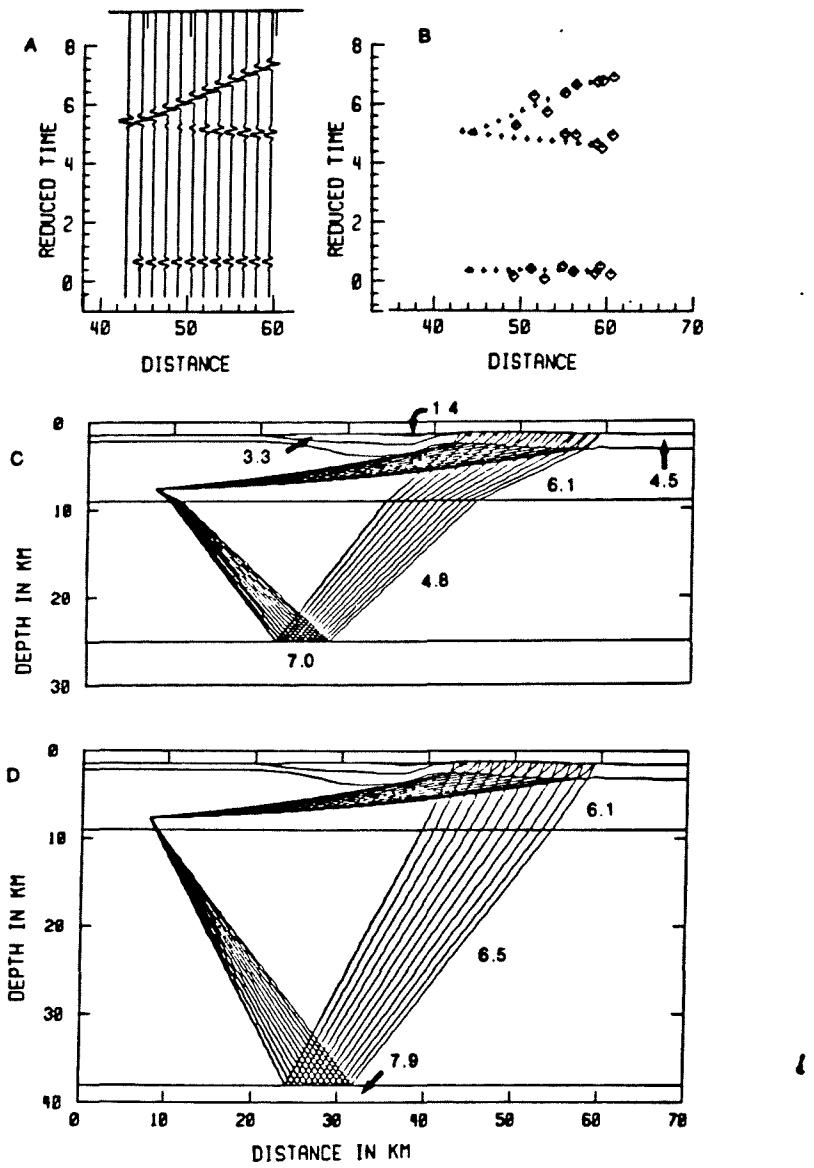

FIG. 4. Model and data for EQ1. (A), (B), and (C) are the synthetic seismogram, travel-time curve, and ray diagram, respectively, for the high-velocity contrast model. (D) is the ray diagram for the simple crustal model. The numbers in the ray diagram indicate layer velocities in kilometers/second. Sea level is at approximately 4 km depth in the model. This model matches the travel times, but does not satisfy the amplitudes.

the *Pr* arrival. As can be seen in Figure 5, this feature also allows us to almost match the amplitude data.

DISCUSSION

These constraints resulted in a LVL that is 21 to 17 km thick under the Long Valley-Mono Craters region. The reflection has to occur on a slightly tilted boundary to match the angle of incidence. This also helps to boost the amplitude of the *Pr* arrival, although it is still somewhat short of producing the required amplitude (Figure 5). A larger *Pr* amplitude could be achieved by lowering the velocity in the

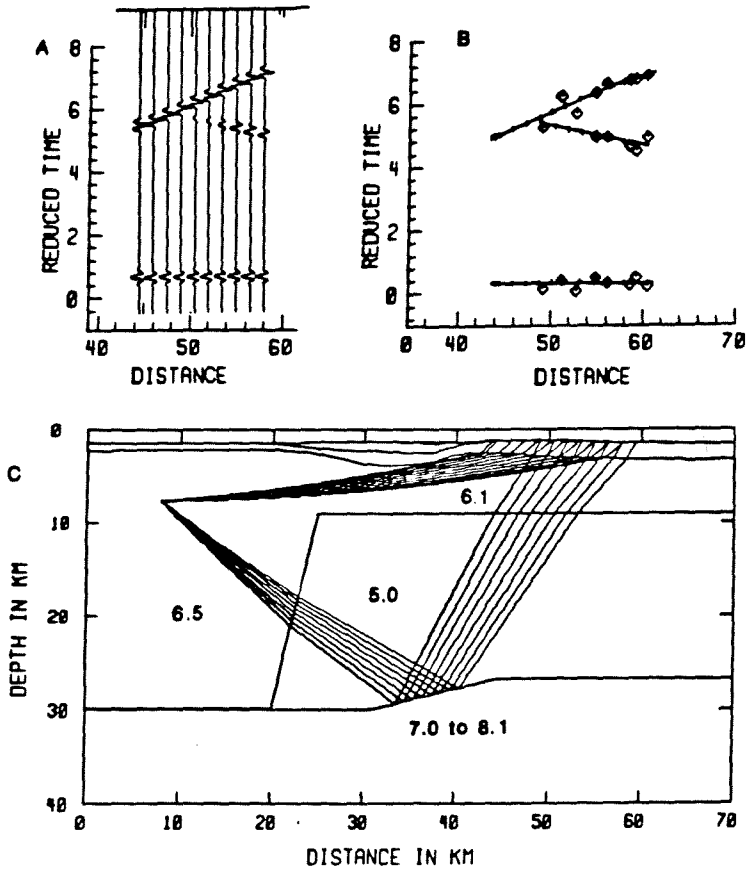

FIG. 5. The two-dimensional model which provides the best fit to the data. (A) Synthetic seismogram calculated for bottom layer of 7.2 km/sec. (B) Travel-time data. (C) Ray diagram. The numbers in the ray diagram indicate layer velocities in kilometers/second. Sea level is at approximately 4 km depth in the model.

LVL, but this would produce a model that was physically unreasonable. This model provides the best fit to our data.

Given that our data set is incomplete and unreversed, we have to rely on other information to constrain the models. The third model illustrates many of the features required to fit the available data. To produce the observed amplitudes, we need to enhance *Pr* by including a low-velocity zone underlain by a high-contrast reflector, a *Pr* take-off angle near 45° from vertical, and a reflector geometry that allows postcritical reflections and focuses many rays toward the reflector. The only free parameter in the amplitude calculation is the velocity at the base of the reflector. We require a velocity above 7.0 km/sec to produce postcritical reflections that approach the correct amplitude. A velocity as high as 8.1 km/sec still produces a reasonable result. To match the travel times with a realistic LVL velocity, the path length in the LVL must be about 35 km, or the overall path must be more convoluted than that shown in Figure 5. To match the incidence angles, either the reflector must tilt to the south or the surface of the LVL must tilt down away from the caldera.

Figure 6 shows the ray paths from our model superimposed on a simplified geologic cross-section after Hill *et al.* (1985b). The geologic cross-section summarizes knowledge about the size of the magma body. As is illustrated in Figure 6, the major

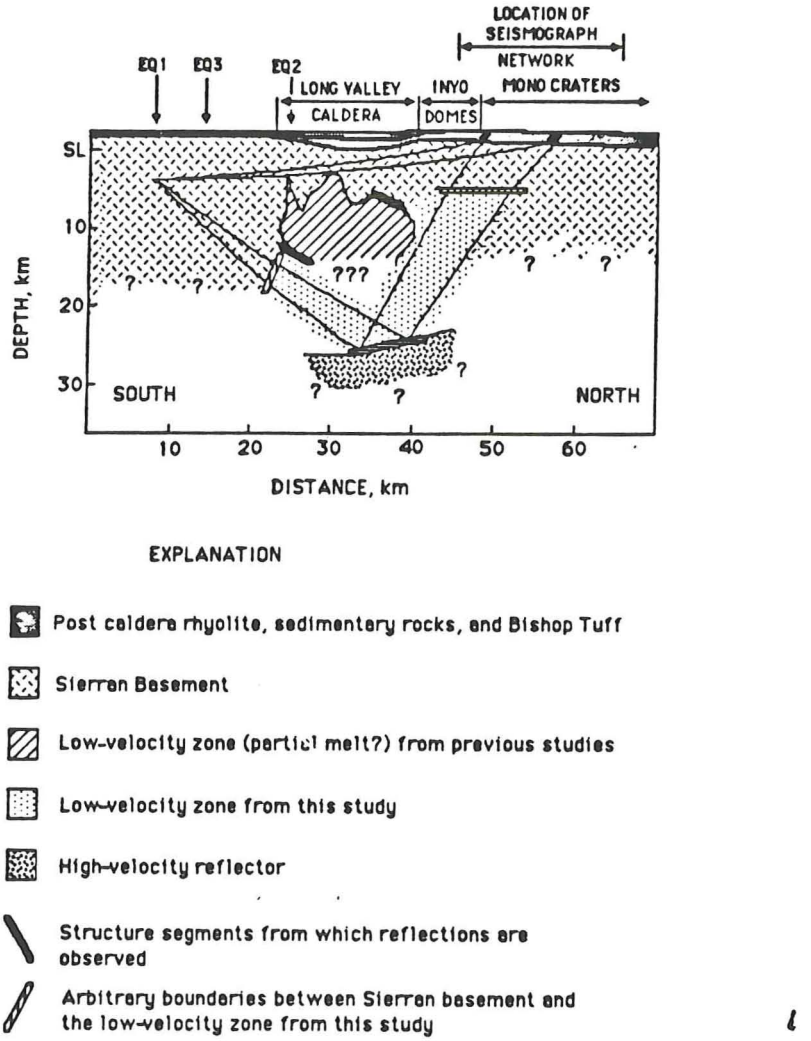

FIG. 6. Geologic interpretation of calculated velocity structure. The low-velocity zone from previous studies is adapted from Rundle *et al.* (1985). The reflector at 25 km distance at 12 km depth is from Luetgert and Mooney (1985). The reflector at 37 km distance and 7 km depth is from Hill (1976). The depth scale is referenced to sea level.

features of our data set are that it requires a much larger magma body than is suggested by Hill *et al.* (1985b) and also requires a high velocity base to the LVL. The LVL that fits our data extends to near the base of the crust and from the southern boundary of the caldera to the Mono Craters area. To make the LVL smaller would require a lower velocity. The velocity in the LVL is not constrained. Some constraint is provided by the amplitudes of the reflection, but in this case, to increase the amplitude of the *Pr* arrival would require lowering of the velocity in the LVL. The velocity contrast is 17 per cent at the top of the LVL. To further increase the contrast would conflict with other studies that have the velocity at approximately 15 per cent or less (Steeples and Iyer, 1976; Kissling *et al.*, 1984; Luetgert and Mooney, 1985).

The main evidence for the thickness/velocity contrast of the LVL comes from the $Pr - P$ time. Our $Pr - P$ time is approximately 2.5 sec greater than Luetgert and Mooney's. Although the point of entry into and exit from the LVL are not well

determined from our data, the large difference in $Pr - P$ times requires the ray paths to pass through a thicker and wider low-velocity zone than is indicated by the "present magma chamber" of Hill *et al.* (1985b). In our model, the LVL extends to 28 km depth, comparable to the depths of basaltic intrusions suggested by Bailey (1982), and consistent with conclusions of Steeples and Iyer (1976) who suggest that magma could exist down to 25 km.

However, in this model, the LVL is wider than the caldera, a somewhat surprising result, but consistent with the recent work of Achauer *et al.* (1986), who suggest that the magma body extends north to the Mono Craters area. If the LVL were constrained to the caldera boundary, then its depth would increase significantly. The unexpected large lateral extent is supported by the fact that to match the travel times we require more than 1-sec delay (in two directions) in the LVL, much larger than observed for one-way, nearly vertical paths, by Steeples and Iyer (1976), 0.35 sec, and Achauer *et al.* (1986), 0.13 sec.

These teleseismic studies see a much smaller delay than is predicted for vertical paths through the model in Figure 5. If the shallow high-velocity material is only found directly beneath the magma body, then reflection paths may be more sensitive to delays in the magma than near-vertical teleseisms, which also pass through the anomalously fast material. Simple one-dimensional analysis based on our model suggest that to explain the teleseismic observations approximately 20 km of excess 7.9 km/sec material is needed beneath the Long Valley area, and approximately 15 km beneath Mono Craters, where the LVL could be much thinner. The detectibility of the high-velocity layers by teleseisms depends on their lateral extent and the ray distribution. However, the detection of a high-velocity reflector deep in the LVL at Long Valley raises questions about past interpretations of teleseismic delays in calderas.

These data have several puzzling features, all indicating that the magma body has a complex shape. Why are our $Pr - P$ times so different from those of Luetgert and Mooney? Rundle *et al.* (1985) show the structure of the low-velocity region beneath the caldera varies considerably. Luetgert and Mooney's reflection could have fortuitously bounced off a different part of the magma chamber. Why is there no *Pr* arrival observed from EQ2 and only the barest hint of it from EQ3? Two factors may contribute to this. First, since EQ3 is shallower and north of EQ1, its rays would strike the reflector at a steeper angle and produce precritical reflections. Rays traced from EQ3 through the model shown in Figure 5 had *Pr* amplitudes reduced by a factor of 2 at the north end of the array and a factor of 10 at the south, compared to *Pr* from EQ1. Presumably, reflections from EQ2 would be even smaller since these rays would be even steeper. Second, the LVL may pinch out west of the ray paths from EQ1 to the receivers. Figure 1 helps support this hypothesis. Thin solid lines connect EQ1 and EQ3 to stations where *Pr* is observed and thin dashed lines connect to stations that did not observe *Pr*. Note that in general the stations on the east side of the network observe *Pr*, whereas the stations on the west side do not. One explanation for this observation is that the LVL is missing under westernmost ray paths from EQ3.

Another puzzling aspect of the data is why EQ2 has poor *S*-wave arrivals. Luetgert and Mooney provide corroborating observations. Their EQ7, which is located near our EQ2, exhibits no *Pr* or *Sg* arrivals. In contrast are their EQ's 1 through 6 which show good *Pr* and *Sg* and which are located approximately 5 km to the east. One explanation for this observation is that a magma cupola of the type inferred by Sanders (1984) is located between EQ2 and the portable network. Furthermore, the

extreme variability of the structure of the LVL (Rundle *et al.*, 1985) can cause focusing and defocusing of energy which could effect the *Pr* arrival. One method for defocusing is to have *Pr* reflect off an inclined boundary under the source as opposed to under the receivers as in Figure 5c. With this geometry, the amplitude of the reflection decreases.

Finally, the model shown in Figure 5 can also be interpreted in terms of the rock types that the velocities represent (Figure 6). The upper two layers, the 1.4, 3.3, and 4.5 km/sec material, probably represent postcaldera rhyolites, sedimentary rocks, and Bishop Tuff within Long Valley (Rundle *et al.*, 1985), and alluvium and weathered basement rocks elsewhere. Rocks of the Sierran basement, which crop out to the west and underlie the area of the profile (Bailey *et al.*, 1976) probably comprise the 6.1 km/sec material. The most likely explanation of the LVL is a region of partial melt associated with a magma chamber. Figure 6 shows the magma chamber existing only in those areas of the velocity model (Figure 5) where the rays actually sample. The rest of the model is shown with question marks. Our interpretation of the LVL is quite similar to that of Luetgert and Mooney (1985), except that our LVL is significantly thicker, and the base of our low-velocity zone is floored with high-velocity material.

The interpretation of the high-velocity material depends on what rock type can be reasonably assigned to a material with velocity greater than 7.0 km/sec. From experimental studies, rocks that have velocities greater than 7.0 km/sec at lower crustal pressures (approximately 10 kb) have a high mafic mineral content (Birch, 1960; Christensen, 1965; Kern and Richter, 1981; Kern, 1982). Candidates include gabbro, amphibolite, and gneiss at velocities approximately 7.0 km/sec and dunite, eclogite, and periodotite at velocities approximately 8.0 km/sec. One possible explanation, therefore, for the high-velocity material is that it represents the upper mantle and that the reflector represents the crustal mantle-boundary. This seems unlikely however, since that would require a crust much thinner than any of the estimates from regional seismic refraction surveys (Eaton, 1966; Prodehl, 1979). Another explanation is that the high-velocity material represents rocks of basaltic (gabbroic) composition that have ponded in the mid-crust during their ascent from the mantle. The injection of basaltic magma into the crust melts the surrounding country rock and is the source for melts of rhyolitic composition (Hildreth, 1981).

Lachenbruch *et al.* (1975) calculate that a minimum of 10 km of basaltic intrusions are required to maintain the Long Valley Caldera system for 2 m.y. Our rough estimates of the thickness of the underplating layer suggest it could be thicker. By combining observations of deep postcritical reflections and teleseismic delays, it may be possible to determine the relative amounts of rhyolitic melt and solidified basaltic magma beneath calderas.

Conclusions

We have performed a passive seismic experiment in the Long Valley Caldera region of California. One earthquake recorded shows a clear, high-amplitude phase arriving between the normal *P* and *S* arrivals. A similar phase has been recorded by other researchers that corroborates our observation. We interpret the phase to be a reflection that has not been significantly laterally refracted. The appearance of this phase is dependent on azimuth which suggests that the reflector is quite heterogeneous. Through amplitude and travel-time modeling, we suggest that the phase, which we call the *Pr* arrival, is a *P* to *P* reflection from the base of a LVL with a high-velocity floor that extends to near the base of the crust.

ACKNOWLEDGMENTS

The authors would like to acknowledge the people who helped make this work possible. Cal Broadwater worked on the field deployment. Lee Younker, Norm Burkhard, and Steve Taylor provided critical reviews of the manuscript and helpful discussions during the research. George Zandt first suggested the effect of high-velocity layer on teleseismic delays. The computer work was done on the Seismic Observatory computers at Lawrence Livermore National Laboratory. Rochelle Hostetter and Liz Garrett speedily typed the many drafts of the manuscript.

This work was performed under the auspices of the U.S. Department of Energy by Lawrence Livermore National Laboratory under Contract W-7405-Eng-48.

REFERENCES

Aki, K. and P. G. Richards (1980). *Quantitative Seismology: Theory and Methods*, vol. 1, W. H. Freeman and Co., San Francisco, California, 557 pages.

Achauer, U., L. Greene, J. R. Evans, and H. M. Iyer (1986). Nature of the magma chamber underlying the Mono Craters area, eastern California, as determined from teleseismic travel time residuals, *J. Geophys. Res.* **91**, 13,873–13,891.

Archuleta, R. J., E. Cranswick, C. Mueller, and P. Spudich (1982). Source parameters of the 1980 Mammoth Lakes, California, earthquake sequence, *J. Geophys. Res.* **87**, 4595–4607.

Bailey, R. A. (1982). Chemical evolution and current state of the Long Valley magma chamber, in *Proceedings of Workshop XIX Active Tectonic and Magmatic Processes Beneath Long Valley Caldera, Eastern California*, D. P. Hill, R. A. Bailey, A. S. Ryall, Editors, *U.S. Geol. Surv., Open-File Rept. 84-939*, 25–40.

Bailey, R. A., G. B. Dalrymple, and M. A. Lanphere (1976). Volcanism, structure, and geochronology of Long Valley Caldera, Mono County, California, *J. Geophys. Res.* **81**, 725–744.

Birch, F. (1960). The velocity of compressional waves in rocks to 10 kilobars. Part 1, *J. Geophys. Res.* **65**, 1083–1102.

Červený, V. and I. Psenčik (1981). SEIS81, a 2-D seismis ray package, Charles University, Prague, Czechoslovakia.

Christensen, N. I. (1965). Compressional wave velocities in metamorphic rocks at pressures to 10 kilobars, *J. Geophys. Res.* **70**, 6147–6164.

Eaton, J. P. (1966). Crustal structure in northern and central California from seismic evidence, in *Geology of Northern California*, E. H. Bailey, Editor, *Calif. Div. Mines Geol. Bull. 190*, 419–426.

Hauksson, E. (1985). Tomographic studies of the Casa Diablo magma chamber using rays from local earthquakes, Long Valley, Eastern California (Abstract), *EOS, Trans. Am. Geophys. Union* **66**, p. 302.

Hildreth, W. (1981). Gradients in silicic magma chambers: implications for lithospheric magmatism, *J. Geophys. Res.* **86**, 10153–10192.

Hill, D. P. (1976). Structure of Long Valley Caldera, California, from a seismic refraction experiment, *J. Geophys. Res.* **81**, 745–753.

Hill, D. P., E. Kissling, J. H. Luetgert, and U. Kradolfer (1985a). Constraints on the upper crustal structure of the Long Valley-Mono craters volcanic complex, eastern California, from seismic refraction measurement, *J. Geophys. Res.* **90**, 11135–11150.

Hill, D. P., R. A. Bailey, and A. S. Ryall (1985b). Active tectonic and magmatic processes beneath Long Valley caldera, eastern California, an overview, *J. Geophys. Res.* **90**, 11,111–11,120.

Johnson, L. R. (1965). Crustal structure between Lake Mead, Nevada, and Mono Lake, California, *J. Geophys. Res.* **70**, 2863–2872.

Kern, H. (1982). *P* and *S* wave velocities in crustal and mantle rocks under the simultaneous action of high confining pressure and high temperature and the effect of the rock microstructure, in *High-Pressure Research in Geoscience*, W. Schreyer, Editor, E. Schweizerbart'sche Verlag, Stuttgart, West Germany, 13–45.

Kern, H. and A. Richter (1981). Temperature derivatives of compressional and shear wave velocities in crustal and mantle rocks at 6 kbar confining pressure, *J. Geophys.* **49**, 47–56.

Kissling, E., W. Ellsworth, and R. S. Cockerham (1984). Three-dimensional structure of the Long Valley, California, region by tomography, in *Proceedings of Workshop XIX Active Tectonic and Magmatic Processes Beneath Long Valley Caldera, Eastern California*, D. P. Hill, R. A. Bailey, A. S. Ryall, Editors, *U.S. Geol. Surv., Open-File Rept. 84-939*, 188–220.

Lachenbruch, A. H., J. H. Sass, R. J. Munroe, and T. H. Moses, Jr. (1976). Geothermal setting and simple heat conduction models for the Long Valley Caldera, *J. Geophys. Res.* **81**.

Lee, W. H. K. and J. C. Lahr (1975). HYPO71 (revised): a computer program for determining hypocenter,

magnitude, and first motion pattern of local earthquakes, *U.S. Geol. Surv., Open-File Rept.75-311*, 111 pp.

Luetgert, J. H. and W. D. Mooney (1985). Crustal refraction profile of the Long Valley Caldera, California, from the January 1983 Mammoth Lakes earthquake swarm, *Bull. Seism. Soc. Am.* **75**, 211–221.

Pitt, A. M. and R. S. Cockerham (1983). Long Valley earthquake swarm, January 7, 1983, *Earthquake Notes* **54**, no. 1, p. 73.

Prodehl, C. (1979). Crustal structure of the western United States, *U.S. Geol. Surv. Profess. Paper 1034*, 74 pp.

Rundle, J. B., G. J. Elbring, R. P. Striker, J. T. Finger, C. C. Carson, M. C. Walck, W. L. Ellsworth, D. P. Hill, P. Malin, E. Tono, M. Robertson, S. Kuhlman, T. McEvilly, R. Clymer, S. B. Smithson, S. Deemer, R. Johnson, T. Henyey, E. Hauksson, P. Leary, J. McCraney, and E. Kissling (1985). Seismic imaging in Long Valley, California, by surface and borehole techniques: an investigation of active tectonics, *EOS, Trans. Am. Geophys. Union* **66**, 194–201.

Rundle, J. B., C. R. Carrigan, H. C. Hardee, and W. C. Luth (1986). Deep drilling to the magmatic environment in Long Valley Caldera, *EOS, Trans. Am. Geophys. Union* **67**, 490–491.

Ryall, F. and A. Ryall (1981). Attenuation of *P* and *S* waves in a magma chamber in Long Valley Caldera, California, *Geophys. Res. Letters* **8**, 557–560.

Sanders, C. O. (1984). Location and configuration of magma bodies beneath Long Valley, California, determined from anomalous earthquake signals, *J. Geophys. Res.* **89**, 8287–8302.

Sanders, C. O. and F. Ryall (1983). Geometry of magma bodies beneath Long Valley, California, determined from anomalous earthquake signals, *Geophys. Res. Letters* **10**, 2597–2609.

Savage, J. C. and M. M. Clark (1982). Magmatic resurgence in Long Valley Caldera, California: possible cause of the 1980 Mammoth Lakes earthquakes, *Science* **217**, 531–533.

Steeples, D. W. and H. M. Iyer (1976). Low-velocity zone under Long Valley as determined from teleseismic events, *J. Geophys. Res.* **81**, 849–860.

LAWRENCE LIVERMORE NATIONAL LABORATORY
P. O. BOX 808
LIVERMORE, CALIFORNIA 94550

Manuscript received 10 July 1986

Note Added in Proof—As this paper went to press, new data was brought to our attention that raises questions about our interpretation. The data were presented by Peppin and Delaplain of the University of Nevada, Reno, at the Long Valley Data Review conference of May 1987 in Berkeley, California. They presented a record section for many earthquakes south of the caldera recorded at station SLK, which is located near our station P12. This record section reverses ours. A striking feature of the data is that *Pr* is clearly observed and has a constant travel-time difference with respect to *Sg*. This implies a negative intercept time suggesting that *Pr* might not be a deep reflection. The model proposed here could change as these new data are interpreted.